

Supplementary Information Section

Structures and Band Gaps of Lead-Free Dabconium-Containing Hybrid Alkali-Metal Halide Perovskites

Hendrik J. van der Poll,^a Rudolph Erasmus,^b Melanie Rademeyer^a

^a Department of Chemistry, University of Pretoria, Pretoria, 0002, South Africa. E-mail: melanie.rademeyer@up.ac.za

^b School of Physics, University of the Witwatersrand, P.O. Wits, 2050 Johannesburg, South Africa

Section 1: Tolerance Factor Calculations

In the parent 3D perovskite structure shown in Figure S1, the A-site cation must fit into the voids of the empty BX_6 -framework, which places geometric restrictions on the combinations of A-, B- and X-ions that will lead to a 3D structure.

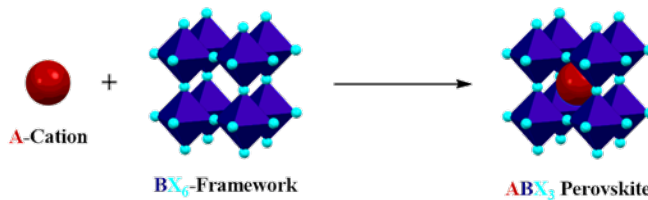


Figure S1. A schematic representation of the formation of a 3D parent perovskite structure. The A-cation (shown as a red sphere) is incorporated in the “voids” of the BX_6 -framework, forming the 3D perovskite structure.

Parameters may be employed to predict if a parent 3D perovskite structure will form for a given combination of A-cation and BX. These include the **Goldschmidt tolerance factor**, t , given in Equation (1),¹ the **octahedral factor**, μ , given in Equation (2)² and Bartell’s tolerance factor,³ τ , given in Equation (3). In these equations, r_i indicates the radius of ion i, and n_A refers to the oxidation state of the A site cation.

When t lies in the range $0.71 < t < 1.05$, a 3D parent perovskite structure is expected. If the tolerance factor lies in the range $0.89 < t < 1$, the cubic 3D phase is predicted, whereas for $0.78 \leq t \leq 0.89$, the more distorted phases such as orthorhombic, rhombohedral or trigonal phases are predicted.^{2,4} Finally, when $0.71 < t \leq 0.78$ or $1.00 < t \leq 1.05$, the tetragonal, hexagonal, or A_4BX_3 -type perovskites are expected.⁵

$$t = \frac{r_A + r_B}{\sqrt{2}(r_B + r_X)} \quad (1)$$

$$\tau = \frac{r_X}{r_B} - n_A \left[n_A - \frac{\left(\frac{r_A}{r_B} \right)}{\ln \left(\frac{r_A}{r_B} \right)} \right] \quad (2)$$

$$\mu = \frac{r_B}{r_X} \quad (3)$$

Values that lie outside this range predict a lower dimensionality perovskite structure. For the octahedral factor, μ , the 3D parent perovskite structure is predicted to be stable in a range of $0.442 \leq \mu \leq 0.895$. Bartel’s tolerance factor is an improved tolerance factor since it also takes the oxidation state of the A-site organic cation into account, and has been shown to correctly predict 92% of 576 materials of the halide and oxide perovskite-types.³ When $\tau < 4.18$, a 3D perovskite structure is predicted.³

The three tolerance factors mentioned previously were calculated for all the compounds of interest, with the results presented in Table S1. The ionic radius of the dabconium dication was taken as 339 pm, as per the determination using Density Functional Theory Calculations reported in the literature.⁶ The Shannon ionic radii⁷ of the metal ions were used. In addition, the structures obtained from the literature survey are also included in Table S1. In the table, tolerance factors that predict a 3D parent perovskite structure are indicated in light grey, whereas those that predict a lower dimensionality are shaded dark grey.

Table S1. Values of tolerance factors, and structures reported in the literature for compounds containing the dabconium cation and alkali metal halides. Light grey indicates the prediction or literature report of a 3D parent perovskite structure while dark grey indicates a structure of lower dimensionality.

Metal Ion (B)	Halide Ion (X)								
	Cl ⁻			Br ⁻			I ⁻		
	t	τ	μ	t	τ	μ	t	τ	μ
Li⁺	1.14	4.35	0.42	1.08	4.55	0.39	0.99	4.86	0.35
	No structure reported			No structure reported			No structure reported		
	1.10	3.31	0.56	1.05	3.46	0.52	0.97	3.69	0.46
Na⁺	No structure reported			No structure reported			No structure reported		
	1.06	2.78	0.76	1.01	2.89	0.70	0.94	3.06	0.63
K⁺	1D hexagonal perovskite (DOTHOK, ⁸ DOTHOK01 ⁹)			3D parent perovskite (FIZYIZ ¹⁰)			No structure reported		
	1.04	2.75	0.84	1.00	2.85	0.78	0.93	3.01	0.69
	3D parent perovskite (GUYNEU, ⁹ GUYNEU01, ¹¹ GUYNEU02 ¹¹)			3D parent perovskite (HEJGUB, ¹¹ HEJGUB01 ¹¹)			1D hexagonal perovskite (HEJHOW ¹¹)		
Rb⁺	1.03	2.82	0.92	0.99	2.91	0.85	0.92	3.05	0.76
	3D parent perovskite (GUYNINY ⁹)			No structure reported			No structure reported		
Cs⁺									

Section 2: Calculated and Experimental Powder X-ray Diffraction (PXRD) Patterns

Experimental PXRD patterns of the bulk samples were compared with powder patterns calculated from the single crystal structures, in order to determine if the single crystal is representative of the bulk sample. The experimental powder patterns are shown in blue and the calculated patterns in red in Figures S2 through S11. Note that these patterns were collected at 298 K and matched with the calculated patterns of crystal structures determined at 150 K, which may lead to a shift in the patterns.

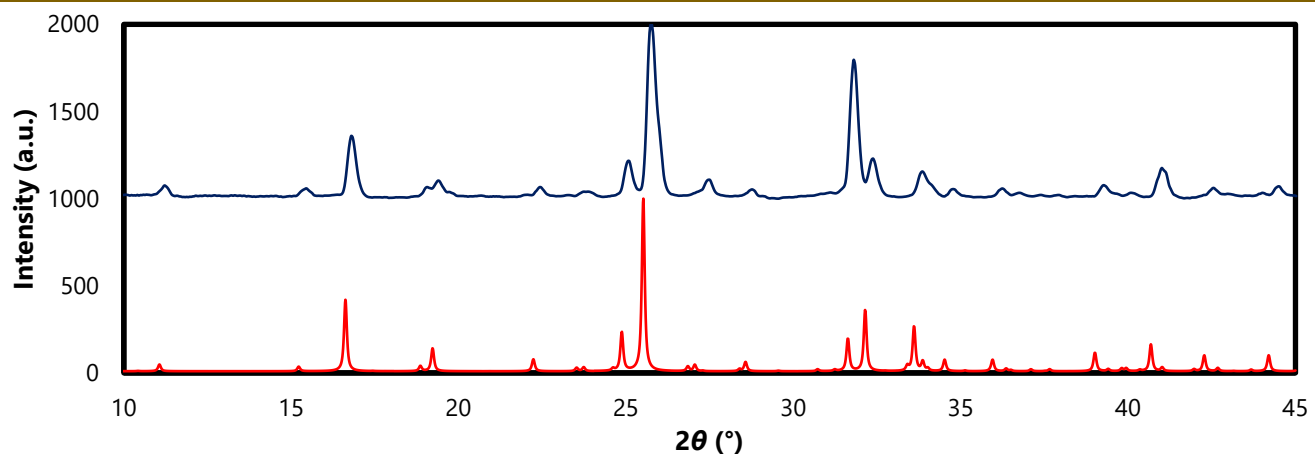


Figure S2. The calculated (red) and experimental (blue) powder patterns for **D-NaCl₃**.

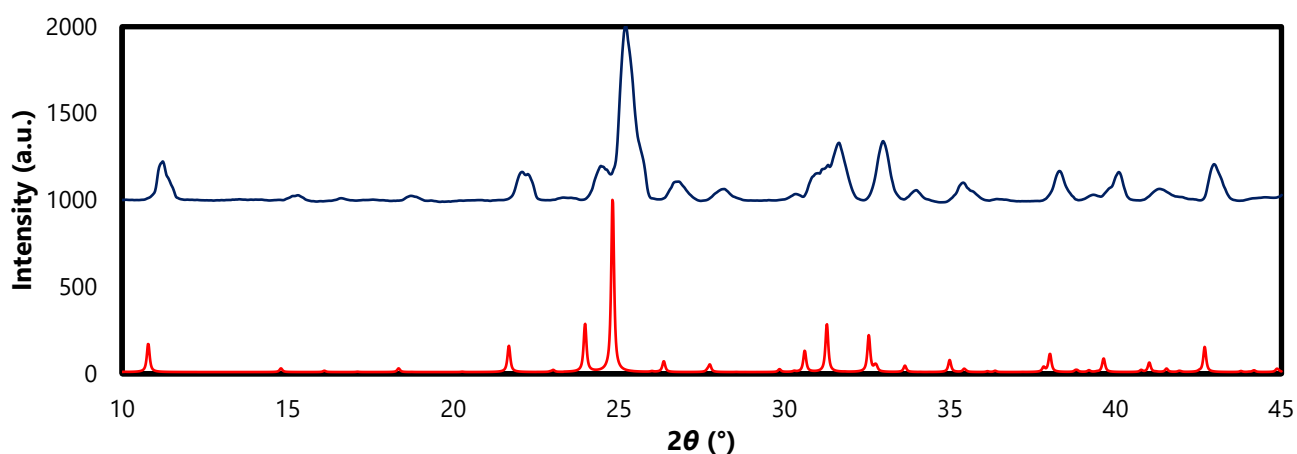


Figure S3. The calculated (red) and experimental (blue) powder patterns for **D-NaBr₃**.

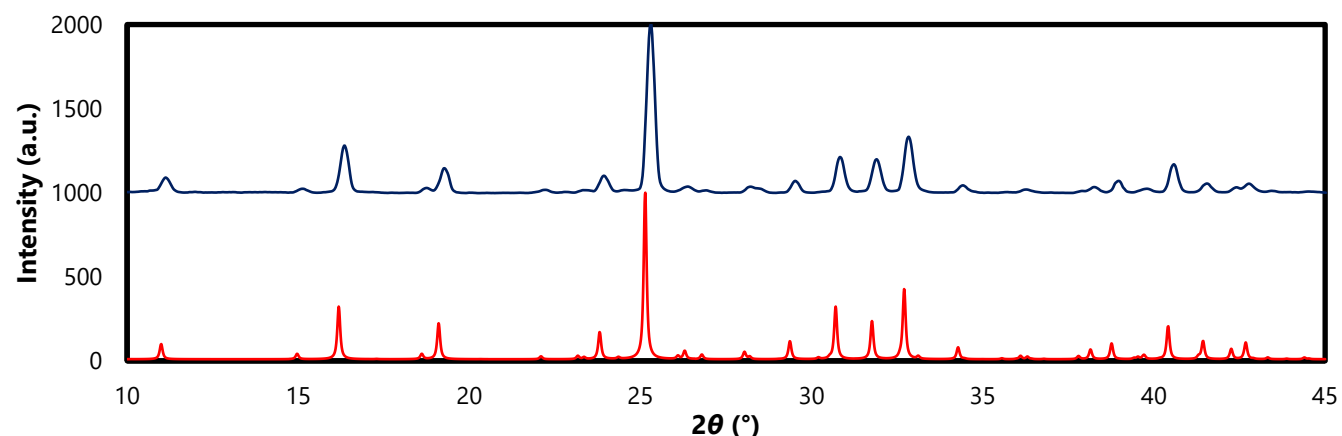


Figure S4. The calculated (red) and experimental (blue) powder patterns for **D-KCl₃**.

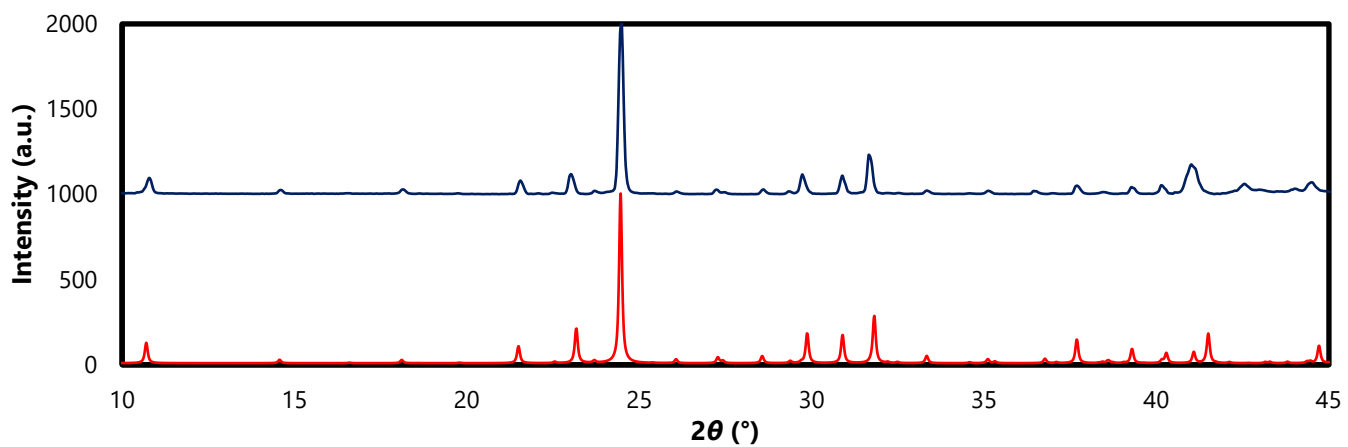


Figure S5. The calculated (red) and experimental (blue) powder patterns for **D-KBr₃(1)**.

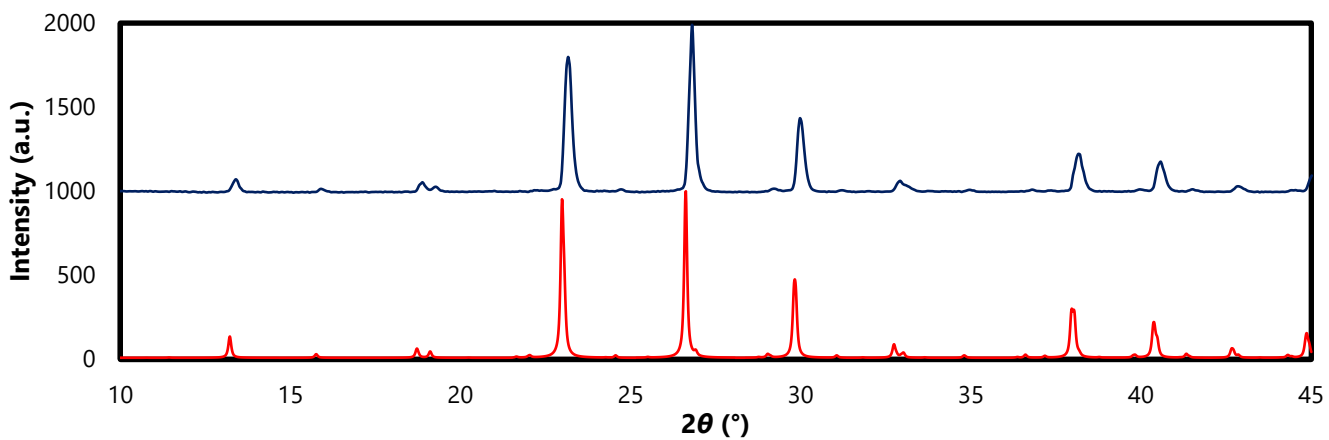


Figure S6. The calculated (red) and experimental (blue) powder patterns **D-KBr₃(2)**.

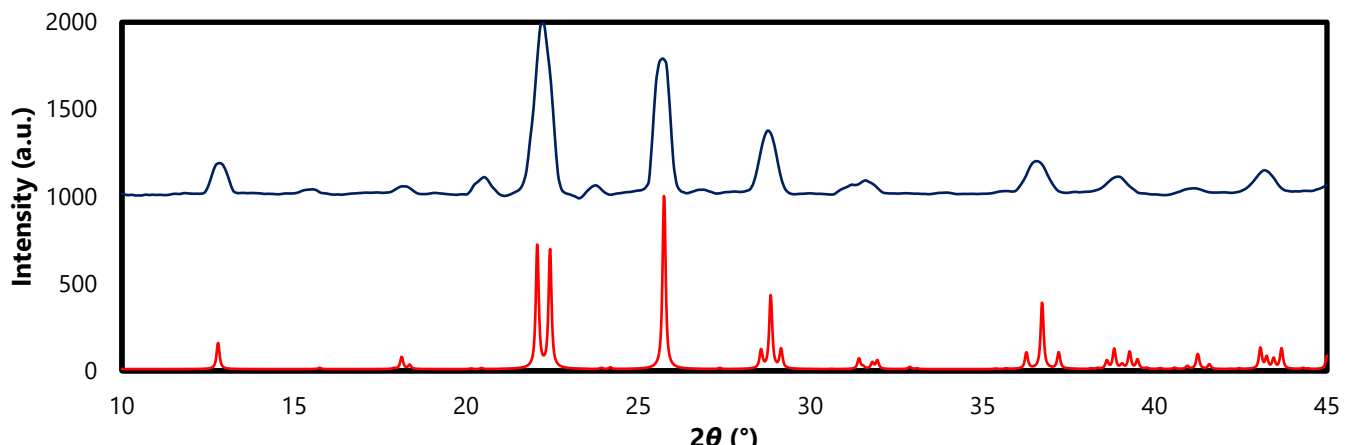


Figure S7. The calculated (red) and experimental (blue) powder patterns for **D-KI₃**.

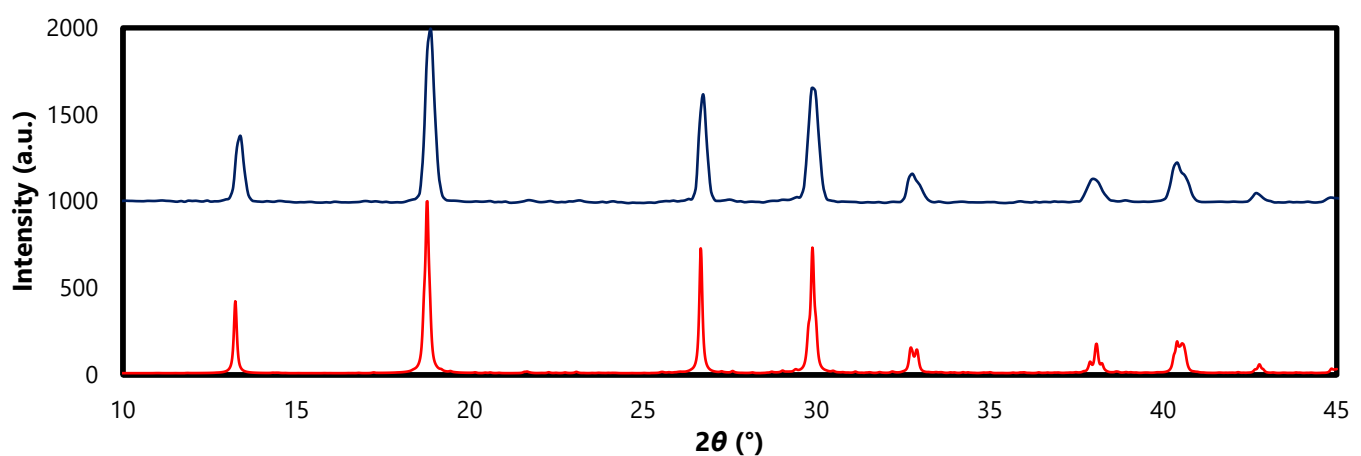


Figure S8. The calculated (red) and experimental (blue) powder patterns **D-CsCl₃**.

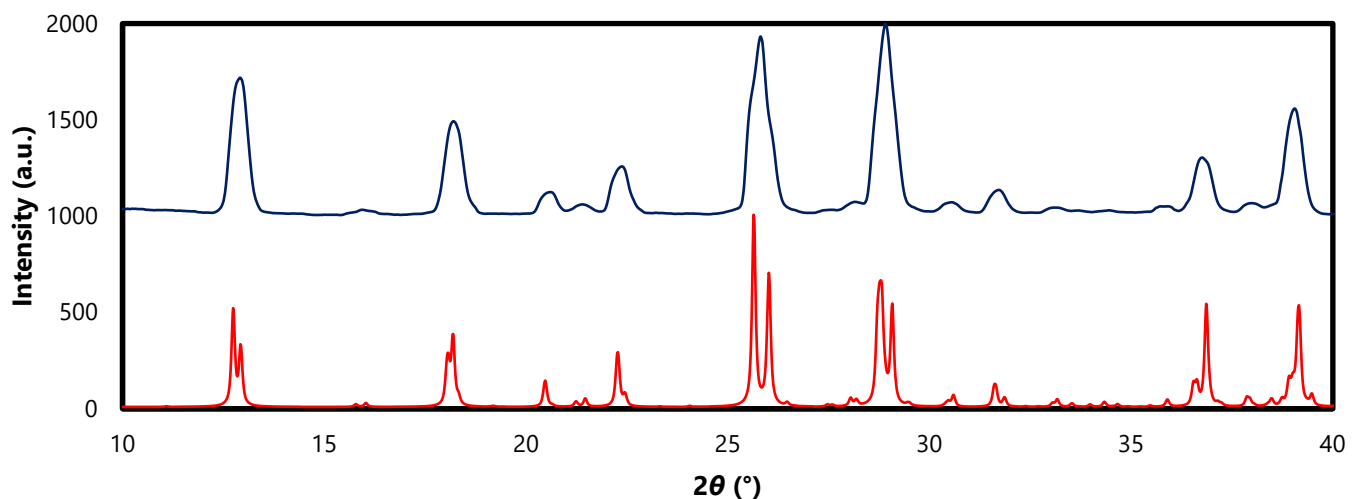


Figure S9. The calculated (red) and experimental (blue) powder patterns for **D-CsBr₃**.

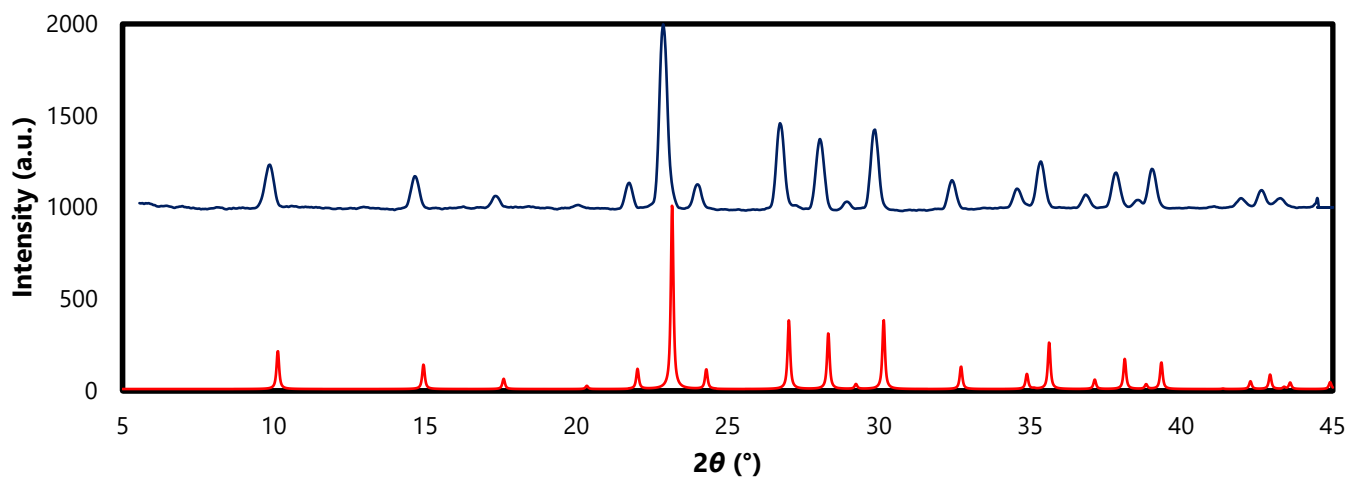


Figure S10. The calculated (red) and experimental (blue) powder patterns for **D-CsI₃**.

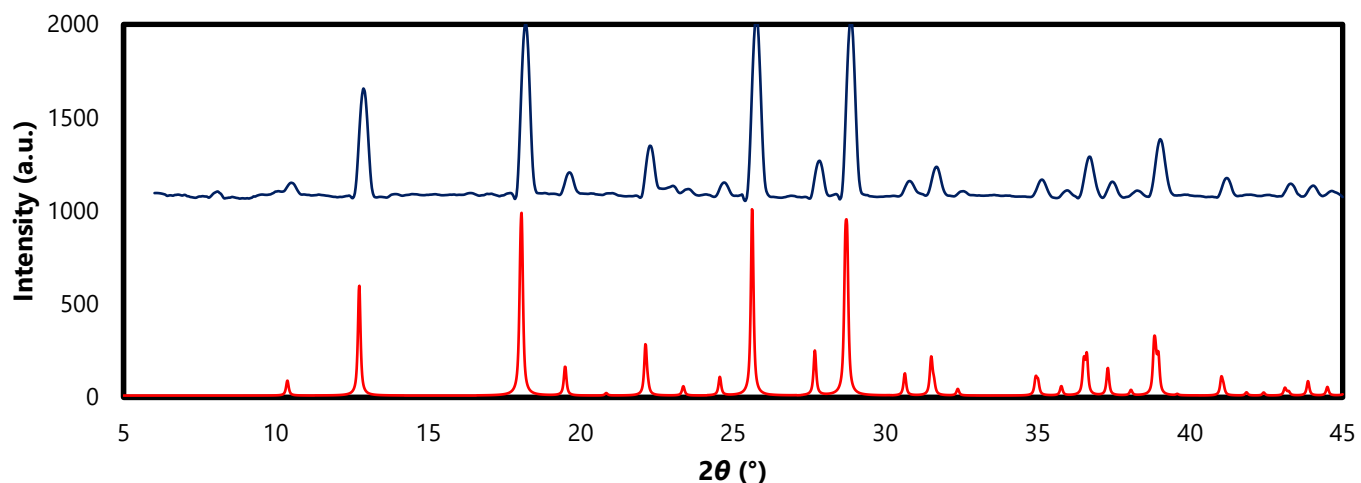


Figure S11. The calculated (red) and experimental (blue) powder patterns for **D**-CsICl₂.

Section 3: Crystallographic and Geometric Parameters

The Tables S2 through S5 provide the crystallographic and geometric parameters of the structures studied here. Table S6 provides the crystallographic information on the literature structures that were included in the comparison.

Table S2. Additional crystallographic parameters of 1D hexagonal perovskite structures.

Structure Abbreviation	D-NaCl ₃	D-NaBr ₃	D-KCl ₃	D-KBr ₃ (1)	D-CsI ₃
Name	<i>catena-[bis(1,4-diazeniabicyclo[2.2.2]octane-1,4-diium) nonakis(μ_2-chloro)-tri-sodium]</i>	<i>catena-[bis(1,4-diazeniabicyclo[2.2.2]octane-1,4-diium) nonakis(μ_2-bromo)-tri-sodium]</i>	<i>catena-[bis(1,4-diazeniabicyclo[2.2.2]octane-1,4-diium) nonakis(μ_2-chloro)-tri-potassium]</i>	<i>catena-[bis(1,4-diazeniabicyclo[2.2.2]octane-1,4-diium) nonakis(μ_2-bromo)-tri-potassium]</i>	<i>catena-[1,4-diazabicyclo[2.2.2]octane-1,4-diium tris(μ_2-iodo)-caesium]</i>
Perovskite Type	1D Hexagonal	1D Hexagonal	1D Hexagonal	1D hexagonal	1D hexagonal
Wavelength (Å)	1.54184	1.54184	0.71073	0.71073	0.71073
Volume (Å ³)	4625.04(7)	5093.19(13)	4947.79(15)	5440.5(2)	696.81(3)
Crystal size (mm ³)	0.09×0.05×0.03	0.15×0.19×0.21	0.06×0.06×0.10	0.13×0.16×0.16	0.17×0.23×0.43
Completeness	1.000	1.000	1.000	1.000	1.000
Parameters	61	57	60	57	17

Table S3. Additional crystallographic parameters of 3D perovskite structures.

Structure Abbreviation	D-KI ₃	D-CsCl ₃	D-CsBr ₃	D-CsICl ₂
Name	<i>catena-[bis(1,4-diazeniabicyclo[2.2.2]octane-1,4-diium) hexakis(μ_2-iodo)-di-potassium]</i>	<i>catena-[tetrakis(1,4-diazeniabicyclo[2.2.2]octane-1,4-diium) dodecakis(μ_2-chloro)-tetra-caesium]</i>	<i>catena-[1,4-diazabicyclo[2.2.2]octane-1,4-diium tris(μ_2-bromo)-caesium]</i>	<i>catena-[1,4-diazabicyclo[2.2.2]octane-1,4-diium di(μ_2-chloro)-(μ_2-iodo)-caesium]</i>
Perovskite Type	3D	3D	3D	3D
Wavelength (Å)	0.71073	0.71073	0.71073	0.71073
Volume (Å ³)	995.21(16)	9536.4(12)	2636.75(12)	989.11(3)
Crystal size (mm ³)	0.065×0.049×0.025	0.10×0.11×0.15	0.08×0.10×0.12	0.11×0.22×0.35
Completeness	1.000	0.887	0.964	1.000
Parameters	17	436	124	56

Table S4. Selected geometric parameters for the 1D hexagonal perovskite structures.

Structure	D-NaCl ₃		D-NaBr ₃		D-KCl ₃		D-KBr ₃₍₁₎		D-RbI ₃ ¹¹	D-CsI ₃
Temperature (K)	150(2)		150(2)		150(2)		150(2)		293(2)	150(2)
B-X (Å)	Na1 2.8812(6) 2.9861(6)	Na2 2.8389(3)	Na1 3.0308(8) 3.1237(9)	Na2 2.9814(2)	K1 3.1297(3) 3.2143(3)	K2 3.08170(19)	K1 3.3533(4) 3.2784(4)	K2 3.22380(17)	3.6698(8)	3.7806(3)
X-B-X (°)	Na1 83.51(2) 88.04(2) 89.590(7) 99.256(7) 172.248(13)	Na2 88.925(10) 91.0 74(10) 180	Na1 84.50(3) 88.45(3) 89.321(5) 98.048(5) 173.074(16)	Na2 89.571(6) 90.427(5) 180	K1 86.371(8) 87.782(4) 89.017(7) 97.224(4) 172.932(4)	K2 88.907(5) 91.093(5) 180.0	K1 173.654(5) 87.135(12) 87.638(3) 89.352(12) 96.195(4)	K2 180 88.398(4) 91.786(13) 91.600(4) 172.585(19)	83.133(19) 93.760(19) 91.786(13) 172.585(19)	85.308(4) 94.692(4) 180
B-X-B (°)	73.28(3) 75.761(15)		74.635(19) 72.71(4)		71.913(10) 72.279(6)		71.392(9) 71.443(18)		67.982(19)	63.742(6)
B···B (Å)	Na1···Na2 3.5785(9)	Na1···Na1 3.4390(17)	Na1···Na2 3.7028(13)	Na1···Na1 3.593(3)	K1···K2 3.6753(6)	K2···K2 3.7147(3)	K1···K2 3.8390(6)	K1···K1 3.8283(12)	4.1033(8)	3.99245(10)
N-H+···X-B (D···A) (Å)	3.0180(12)		3.1734(16)		3.0256(7)		3.1852(14)		3.256	3.773(4)

Table S5. Selected geometric parameters for the 3D parent perovskite structures.

Structure	D-KBr₃(2)¹⁰	D-KI₃	D-RbCl₃(1)⁹		D-RbBr₃(1)¹¹	
Structure Type	3D Perovskite	3D Perovskite	3D Perovskite		3D Perovskite	
Temperature (K)	283-303	150(2)	120(2)		293(2)	
B-X (Å)	3.331	3.4732(2)	Rb1	Rb2	Rb1	Rb2
	3.332		3.2924(7)	3.2894(8)	3.3990(17)	3.3863(13)
	3.346		3.3040(8)	3.3198(8)	3.4070(16)	3.4275(17)
	3.347		3.3179(8)	3.2899(8)	3.4374(13)	3.4439(17)
X-B-X (°)	172.02	85.29(4)	Rb1	Rb2	Rb1	Rb2
	172.12		78.919(19)	82.716(18)	83.26(3)	80.16(3)
	166.68		83.22(3)	84.68(3)	84.69(5)	84.35(3)
	86.77		85.01(2)	86.222(18)	86.34(3)	85.07(5)
	84.25		89.15(3)	88.140(18)	87.74(3)	88.53(5)
	94.01		94.441(19)	93.405(19)	93.49(3)	94.51(4)
	85.36		96.023(18)	97.44(2)	97.16(3)	95.26(3)
	95.57		101.322(19)	102.88(3)	102.63(6)	100.83(4)
	84.25		163.79(2)	165.32(3)	165.58(6)	164.48(3)
	101.09		171.20(3)	170.90(2)	171.03(5)	172.83(6)
B-X-B (°)	173.51	170.93(6)	161.35(3)		162.18(5)	
	173.80		165.24(3)		165.74(4)	
			172.08(3)		173.03(5)	
N-H+…X-B (D…A) (Å)	N/A	N/A	3.034(3)		2.282	
			3.040(3)		2.244	

Table S5. (Continued) Selected geometric parameters for the 3D parent and hexagonal perovskite structures.

Structure Abbreviation	D-CsCl ₃					D-CsBr ₃ [*]		D-CsICl ₂	
Structure Type	3D Perovskite					3D Perovskite		3D Perovskite	
Temperature (K)	150(2)					150(2)		150(2)	
B-X (Å)	Cs1	Cs2	Cs3	Cs4	Cs5	Cs1	Cs2	Cl1	I1
	3.3630(5)	3.3324(4)	3.3343(5)	3.3351(5)	3.3444(4)			3.3828(8)	
	3.3937(5)	3.3496(5)	3.3392(6)	3.3362(5)	3.4085(5)	3.4574(4)	3.4378(4)	3.4148(7)	
	3.4163(5)	3.3946(5)	3.4179(5)	3.3887(5)	3.4216(5)	3.4996(6)	3.5500(5)		
	3.3977(5)	3.4252(5)	3.4113(5)			3.5042(6)	3.5608(5)		
	3.4183(5)	3.4259(5)	3.4121(5)						
X-B-X (°)	Cs1	Cs2	Cs3	Cs4	Cs5	Cs1	Cs2	Cl1	I1
	179.999(19)							79.75(3)	
	94.616(13)	86.623(13)	97.269(13)	97.616(12)	170.009(17)	79.64(4)	83.277(13)	95.132(5)	
	85.385(14)	93.471(12)	78.079(11)	91.031(13)	91.617(11)	85.75(2)	89.752(13)	97.67(2)	
	85.385(14)	89.310(14)	86.483(14)	83.822(11)	96.427(11)	88.87(2)	89.919(4)	163.30(3)	
	94.614(13)	92.098(12)	88.912(12)	100.501(14)	96.426(11)	89.623(5)	90.081(4)		
	179.999(18)	100.471(14)	84.909(14)	88.536(12)	91.618(11)	91.02(2)	90.248(13)		Cl1 & I1
	91.032(13)	169.015(12)	163.361(11)	166.932(11)	72.821(16)	95.49(2)	96.723(13)		
	88.967(13)	82.955(11)	88.290(12)	165.055(13)	93.059(12)	101.14(3)	180		
	99.343(11)	165.923(12)	173.483(12)	96.114(11)	80.451(12)	169.2(3)			
	80.657(11)	81.928(13)	91.366(13)	84.597(13)	166.360(11)	171.52(2)			
	88.968(12)	89.375(13)	98.647(13)	85.700(14)	93.914(12)				
	91.033(13)	172.520(11)	166.817(12)	84.085(12)	80.451(12)				
	80.657(11)	99.353(13)	92.413(13)	177.962(11)	93.059(12)				
	99.343(11)	91.110(12)	93.674(11)	97.294(11)	93.915(13)				
	180	82.435(12)	100.885(12)	90.051(11)	166.361(11)				
		91.849(12)	81.578(11)	82.314(11)	99.493(17)				
B-X-B (°)	160.951(15)		161.737(15)		158.545(16)				
	157.469(15)		159.284(15)		164.339(15)				
	155.242(14)		160.575(16)		161.119(15)		164.632(19)	154.905(17)	
	167.730(16)		162.351(18)		157.745(18)			165.761(19)	
N-H ⁺ ...X-B (D ^{...} A) (Å)	3.0227(16)		3.0171(17)		3.0523(16)		3.0242(16)		Cl1
	3.0453(16)		3.0374(16)		3.0248(16)		3.222(4)	3.193(4)	3.024(3)
	3.0038(17)								

*Note that only the Br atoms with the highest occupancy are considered.

Table S6. Full crystallographic information of the rubidium structures not synthesised in this study, as well as structure **D-KBr₃(2)**.¹⁰

Structure Abbreviation	D-RbCl₃(1) ⁹	D-RbBr₃(1) ¹¹	D-RbI₃ ¹¹	D-KBr₃(2) ¹⁰
Perovskite Structure Type	3D	3D	1D hexagonal	3D
Empirical Formula	$2n(\text{C}_6\text{H}_{14}\text{N}_2)^{2+} \cdot n[\text{Cl}_6\text{Rb}_2]^{4-}$	$2n(\text{C}_6\text{H}_{14}\text{N}_2)^{2+} \cdot n[\text{Br}_6\text{Rb}_2]^{4-}$	$n(\text{C}_6\text{H}_{14}\text{N}_2)^{2+} \cdot n[\text{RbI}_3]^{2-}$	$2n(\text{C}_6\text{H}_{14}\text{N}_2)^{2+} \cdot n(\text{K}_2\text{Br}_6)^4$
Crystal System	Trigonal	Trigonal	Hexagonal	Trigonal
Space Group	<i>P</i> 3 ₂ 1	<i>P</i> 3 ₂ 1	<i>P</i> 6 ₂ <i>c</i>	<i>P</i> 3 ₁ 21
Temperature (K)	120(2)	293(2)	293(2)	300 K
Wavelength (Å)	0.71073	0.71073	0.71073	-
a (Å)	9.3376(1)	9.6444(14)	9.821(2)	9.47557(6)
b (Å)	9.3376(1)	9.6444(14)	9.821(2)	9.47557(6)
c (Å)	22.3386(5)	23.254(5)	8.2067(16)	23.13707(16)
α (°)	90	90	90	90
β (°)	90	90	90	90
γ (°)	120	120	120	120
Volume (Å³)	1686.77(5)	1873.2(7)	685.5(3)	1799.08
Z	6	6	2	3
Density Calculated (g·cm⁻³)	1.808	2.337	2.812	-
Absorption Coefficient (mm⁻¹)	5.069	13.522	10.330	-
F(000)	912	1236	520	-
Crystal Size (mm³)	0.39×0.33×0.21	0.22×0.18×0.15	0.20×0.12×0.10	-
Reflections Collected	15718	12709	4516	-
Unique Reflections / R_{int}	2586 / 0.0544	2875 / 0.0960	565 / 0.1006	-
Completeness	0.997	0.997	0.985	-
Parameters	8	110	23	-
Flack Parameter	0.009(9)	0.04(3)	-	-
Goodness-of-fit F²	1.032	1.110	1.052	-
Final R indices [I>2σ(I)], (R₁ / wR₂)	0.0349 / 0.0638	0.0652 / 0.1127	0.0279 / 0.0609	6.88
R indices (all data), (R₁ / wR₂)	0.0517 / 0.0680	0.1040 / 0.1241	0.0284 / 0.0611	-

S4 Structural Trends

S4.1 Comparison of 1D Hexagonal Perovskite Structures

The spread of the structural parameters of the 1D hexagonal perovskite structures is provided in Table S7. This table is used in the discussion of the structural trends section in the main text.

Table S7. Spread of structural parameters obtained for the 1D hexagonal perovskite structures.

Structure	$B^+ + X^-$ Ionic Radii (pm)	Δd (Å)	$\Delta(B \cdots B)$ (Å)	$\Delta(B-X-B)$ (°)	$\Delta(X-B-X)$ (°)		Average Spread
					Equatorial	Axial	
D-NaCl ₃	283	4.5×10^{-4}	4.0×10^{-4}	2.8×10^{-4}	2.8×10^{-3}	4.8×10^{-4}	8.7×10^{-4}
D-NaBr ₃	298	3.7×10^{-4}	2.2×10^{-4}	1.7×10^{-4}	2.0×10^{-3}	3.9×10^{-4}	6.3×10^{-4}
D-KCl ₃	319	2.6×10^{-4}	5.2×10^{-6}	1.39×10^{-6}	1.5×10^{-3}	4.2×10^{-4}	4.3×10^{-4}
D-KBr ₃ (1)	334	2.6×10^{-4}	1.9×10^{-6}	1.59×10^{-7}	1.2×10^{-3}	3.2×10^{-4}	3.5×10^{-4}
D-RbI ₃ ¹¹	372	0	0	0	1.3×10^{-3}	0	2.7×10^{-4}
D-CsI ₃	387	0	0	0	9.1×10^{-4}	0	1.8×10^{-4}

S4.2 Comparison of 3D Perovskite Structures

The spread of the structural parameters of the 3D perovskite structures are provided in Table S8. This table is used in the discussion of the structural trends section in the main text.

Table S8. Spread of structural parameters for the 3D dabconium-containing perovskite structures.

Structure	$B^+ + X^-$ Ionic Radii (pm)	Δd (Å)	$\Delta(B-X-B)$ (°)	$\Delta(X-B-X)$ (°)		Average Spread	Phase	Space Group
				Equatorial	Axial			
D-KBr ₃ (2)	334	0	0	2.4×10^{-3}	0	6.1×10^{-4}	Trigonal	P3 ₁ 21
D-KI ₃	358	0	0	1.5×10^{-3}	0	3.7×10^{-4}	Trigonal	R32
D-RbCl ₃ (1) ⁹	333	1.5×10^{-5}	7.1×10^{-4}	6.2×10^{-3}	3.9×10^{-4}	1.8×10^{-3}	Trigonal	P3 ₂ 21
D-RbBr ₃ (1) ¹¹	348	3.7×10^{-5}	7.3×10^{-4}	5.6×10^{-3}	4.4×10^{-4}	1.7×10^{-3}	Trigonal	P3 ₂ 21
D-CsCl ₃	348	1.2×10^{-4}	4.0×10^{-4}	5.4×10^{-3}	8.7×10^{-4}	1.7×10^{-3}	Monoclinic	C2/c
D-CsBr ₃	363	1.6×10^{-4}	9.1×10^{-4}	3.5×10^{-3}	7.1×10^{-4}	1.3×10^{-3}	Orthorhombic	Pbcn
D-CsCl ₂ I ^a	361	1.9×10^{-3}	3.6×10^{-4}	4.8×10^{-3}	5.9×10^{-4}	1.9×10^{-3}	Trigonal	P3 ₁ 21

^a The sum of the radii of D-CsCl₂I was taken as $r_{\text{Sum}} = r_{\text{Cs}^+} + \frac{2}{3}r_{\text{Cl}^-} + \frac{1}{3}r_{\text{I}^-}$

S5 Evaluation of the Success of Prediction Factors

In Tables S9 and S10 the success of the prediction factors discussed in the main text are visually illustrated.

Table S9. Combinational evaluation of the success of the predictions of the tolerance factors. Green blocks indicate successful prediction by at least one factor, whereas red blocks indicate a complete failure of all the factor's prediction.

		Cl ⁻	Br ⁻	I ⁻
Na ⁺	Obtained	1D	1D	?
	Predicted	1D or 3D	3D	3D
K ⁺	Obtained	1D	1D and 3D	3D
	Predicted	1D or 3D	3D	3D
Cs ⁺	Obtained	3D	3D	1D
	Predicted	1D or 3D	3D	3D

Table S10. Evaluation of the success of the individual predictions of the tolerance factors. Green blocks indicate successful prediction, whereas red blocks indicate a complete failure of the factor's prediction, and blue blocks indicate a mixture where neither can be assigned as “correctly” or “incorrectly” predicted. Grey indicates that no structure was obtained.

Metal Ion (B)	Halide Ion (X)								
	Cl ⁻			Br ⁻			I ⁻		
	<i>t</i>	τ	μ	<i>t</i>	τ	μ	<i>t</i>	τ	μ
Na⁺	1.10	3.31	0.56	1.05	3.46	0.52	0.97	3.69	0.46
	1D structure obtained			1D structure obtained			No structure obtained		
K⁺	1.06	2.78	0.76	1.01	2.89	0.70	0.94	3.06	0.63
	1D structure obtained			1D and 3D structures obtained			3D structure obtained		
Cs⁺	1.03	2.82	0.92	0.99	2.91	0.85	0.92	3.05	0.76
	3D structure obtained			3D structure obtained			1D structure obtained		

S6 Interpretation of Diffuse Reflectance Spectra via Kubelka-Munk Theory

According to the Kubelka-Munk theory, the reflectance data of an infinitely thick specimen can be converted to absorbance data by use of the Kubelka-Munk remission function ($F(R_\infty)$), as follows¹²⁻¹⁴

$$F(R_\infty) = \frac{K}{S} = \frac{(1 - R_\infty)^2}{2R_\infty} \quad (4)$$

where $R_\infty = \frac{R_{\text{sample}}}{R_{\text{standard}}} = \frac{\%R}{100}$ is related to the percentage reflectance of the material, while K and S are the absorption and scattering coefficients, respectively.¹² Furthermore, the Tauc method assumes that the absorbance, and hence the energy-dependent absorbance coefficient (α) of the crystalline material may be expressed as shown in Equation (5)

$$(\alpha \cdot h\nu)^{\frac{1}{\gamma}} = B(h\nu - E_g) \quad (5)$$

where h is the Planck constant, ν is the photon's frequency, E_g is the band gap energy, and B is a constant. If the transition is *direct*, then $\gamma = 0.5$, and if the transition is *indirect*, then $\gamma = 2$.¹⁵ Therefore, by combining Equation (5) with the expression for $F(R_\infty)$, the result is Equation (6)

$$(F(R_\infty) \cdot h\nu)^{\frac{1}{\gamma}} = B(h\nu - E_g) \quad (6)$$

Hence, by plotting $(F(R_\infty) \cdot h\nu)^{1/\gamma}$ against $h\nu$, the band gap (E_g) can be determined by extrapolating the linear part of the function and determining its intersection with the x -axis. γ is taken as 0.5 for all dabconium containing materials since they all exhibit only one absorption edge and hence possess direct band gaps. The DRS data collected for the dabconium-containing materials were processed, and the lines of best fit of the linear parts were determined.

The raw data obtained from the diffuse reflectance spectrometer has a percentage reflectance associated with a given radiation wavelength. The percentage reflectance is then converted to a fraction of 1 so that the parameters K and S may be calculated. Following this, the value of the Kubelka-Munk remission function, $F(R_\infty)$, is calculated using the K and S values. Finally, the photon energy is calculated from the wavelength of the radiation ($E = \frac{hc}{\lambda}$, to be used as the x -axis variable) and $(F(R_\infty) \cdot h\nu)^2$ is calculated as the y -axis variable (the Planck constant was taken as $h = 6.626 \times 10^{-34}$ J·s and the speed of light as $c = 2.99792458 \times 10^8$ m·s⁻¹).

$(F(R_\infty) \cdot h\nu)^{1/\gamma}$ is plotted against $h\nu$, and two linear regions are typically identified. The first transition occurs as a phonon-assisted transition (photon + phonon) and the second from a photon-only transition. Therefore, the first (lower energy) transition corresponds to the indirect optical band gap and the linear region where the tangent line will be calculated from. The tangent line is then drawn to the linear region. The equation of this line is determined by regression analysis. The indirect optical band gap of the sample is given by the intercept of the tangent line with the x -axis of the graph. The parameters for the direct transition are calculated in the same ways as for the indirect transition, except that the second absorption edge is considered.

S5.1 Original DRS Spectra

The original DRS spectra for the compounds are given in Figure S12.

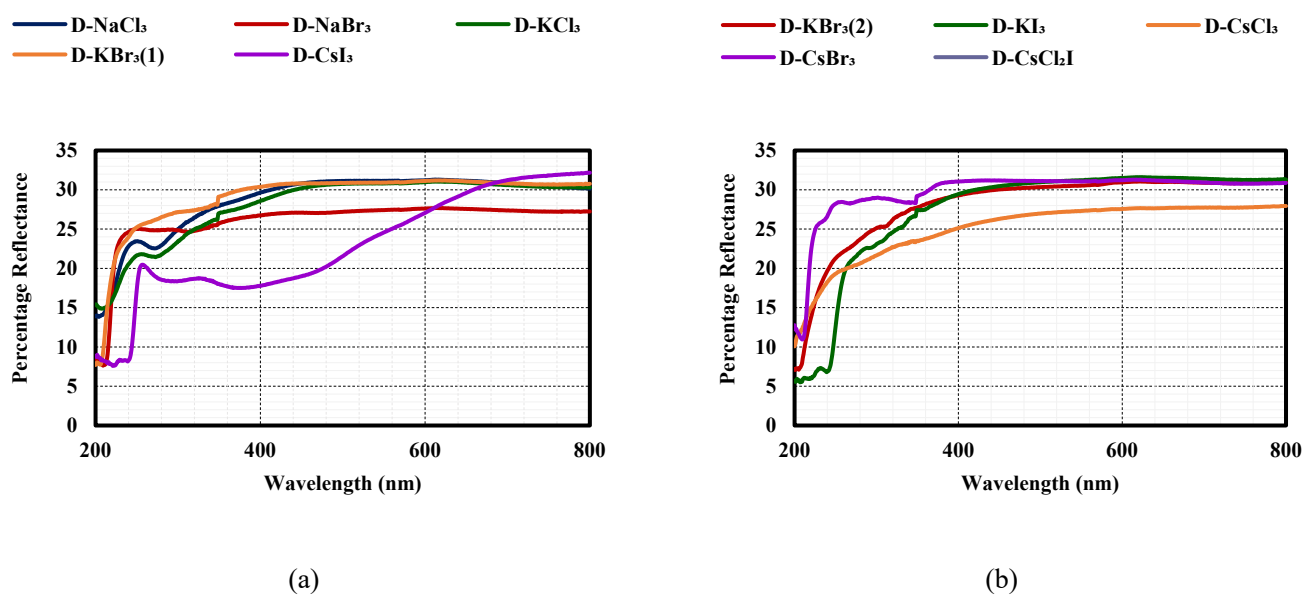


Figure S12. The reflectance data obtained from the DRS analysis plotted against radiation wavelength for (a) the 1D ABX₃-type dabconium-containing perovskite materials, (b) the 3D dabconium-containing perovskite materials.

References

- 1 V. M. Goldschmidt, *Naturwissenschaften*, 1926, **14**, 477–485.
- 2 X. L. Chonghea Li, L. F. Weizhong Ding and Z. G. Yonghui Gao, *Acta Crystallographica Section B*, 2008, **64**, 702–707.
- 3 C. J. Bartel, C. Sutton, B. R. Goldsmith, R. Ouyang, C. B. Musgrave, L. M. Ghiringhelli and M. Scheffler, *Science Advances*, 2018, **2**, 1–10.
- 4 T. T. Ava, A. Al Mamun, S. Marsillac and G. Namkoong, *Applied Sciences (Switzerland)*, 2019, **9**, 188.
- 5 W. F. Yang, F. Igbari, Y. H. Lou, Z. K. Wang and L. S. Liao, *Advanced Energy Materials*, 2020, **10**, 1–30.
- 6 C. Shi, H. Yu, Q. Wang, L. Ye, Z. Gong, J. Ma, J. Jiang, M. Hua, C. Shuai, Y. Zhang and H. Ye, *Angewandte Chemie*, 2020, **132**, 173–177.
- 7 R. D. Shannon, *Acta Crystallographica Section A*, 1976, **32**, 751–767.
- 8 F. Thétiot, I. Sasaki, C. Duhayon and J. P. Sutter, *Journal of Chemical Crystallography*, 2009, **39**, 225–227.
- 9 L. A. Paton and W. T. A. Harrison, *Angewandte Chemie*, 2010, **49**, 7684–7687.
- 10 H. Zhang, *CSD Private Communication*.
- 11 W. Y. Zhang, Y. Y. Tang, P. F. Li, P. P. Shi, W. Q. Liao, D. W. Fu, H. Y. Ye, Y. Zhang and R. G. Xiong, *Journal of the American Chemical Society*, 2017, **139**, 10897–10902.
- 12 R. López and R. Gómez, *Journal of Sol-Gel Science and Technology*, 2012, **61**, 1–7.
- 13 M. Nowak, B. Kauch and P. Szperlich, *Review of Scientific Instruments*, 2009, **80**, 21–24.
- 14 P. Kubelka and M. Franz, *Technical Physics*, 1931, **19**, 593–601.
- 15 J. I. Pankove and D. A. Kiewit, *Journal of The Electrochemical Society*, 1975, **119**, 156.